OPEN ACCESS

University of BRISTOL

Peer reviewed version

Link to published version (if available):
10.1063/1.5047911

Link to publication record in Explore Bristol Research
PDF-document

University of Bristol - Explore Bristol Research
General rights

Perspective: The development and applications of H Rydberg atom translational spectroscopy methods

Michael N.R. Ashfold,[1] Kaijun Yuan [2] and Xueming Yang [2]

[1] School of Chemistry, University of Bristol, Bristol, U.K. BS8 1TS

[2] State Key Laboratory of Molecular Reaction Dynamics, Dalian Institute of Chemical Physics, Chinese Academy of Sciences, 457 Zhongshan Road, Dalian, 116023, China

Abstract

Determining the product velocities offers one of the most direct and penetrating experimental probes of the dynamics of gas phase molecular photodissociation and bimolecular collision processes, and provides an obvious point of contact with theoretical molecular dynamics simulations, potential energy surfaces, and non-adiabatic couplings between such surfaces. This Perspective traces the development of the H Rydberg atom translational spectroscopy technique from a serendipitous first encounter through to the present, highlights the advances that make it the method of choice for studying many benchmark photofragmentation and photoinduced collision processes that yield H (or D) atoms amongst the products, and anticipates some future opportunities afforded by the technique.

Introduction

A recent Perspective [1] prefacing a special issue devoted to advanced particle imaging highlighted the ever growing impact of velocity map imaging methods [2] in improving our knowledge and understanding of the dynamics of gas phase chemical reactions. It also reminds us of the important but unpredictable ways in which scientific advances can be stimulated by chance encounters between individuals with complementary interests and expertise. The concept of ion imaging as a way of obtaining correlated quantum state specific information about products formed in a molecular photodissociation process emerged from conversations between Dave Chandler and Paul Houston at Faraday Discussion 82 in Bristol in 1986. The first demonstration of the technique was reported the following year. [3]

One of the present authors also contributed to a paper presented at that Discussion. [4] The paper reported the first demonstration of another photofragment translational spectroscopy (PTS) method, which has also had a major impact within the reaction dynamics community. The birth of this method can be traced to a similarly serendipitous encounter, between Karl Welge and Mike Ashfold on a bus returning delegates from the 1984 Gordon Research Conference (GRC) on Multiphoton Processes to Logan Airport in Boston. Welge was already internationally renowned for his development and application of tuneable vacuum ultraviolet (VUV) light sources in several areas of fundamental chemical physics. Ashfold, in contrast, was just starting out. This was his first GRC, at which he presented detailed new insights into the predissociation mechanisms of gas phase water molecules gleaned from analysing and simulating resonance enhanced multiphoton ionization (REMPI) spectra of both H_2O and D_2O. [5] The electronic absorption of water lies in the VUV spectral region, and the predissociating states studied in the REMPI experiments lie at excitation energies ~10 eV. Hard though it may now be to believe, the predissociation products were at that time still unclear. Electronically excited OH(A) photofragments had been identified following photoexcitation at such energies. [6] Analysis of their spontaneous fluorescence showed that these fragments were formed with high levels of rotational excitation, but quantum yield estimates [7] suggested that they amounted to no more than 10% of the total dissociation yield. Theory suggested that O–H bond fission leading to ground state OH(X) products must be the main fragmentation pathway, but all attempts to detect such products up to that time had been unsuccessful. The conversation on the bus suggested a new way of settling this issue, and Ashfold spent the following summer as a visitor in Welge's group at Universität Bielefeld helping to implement the idea.
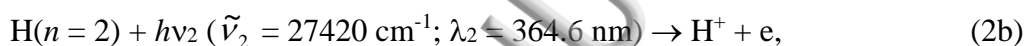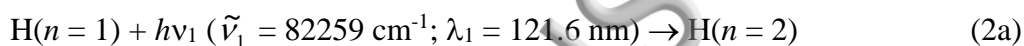
The early days of H atom photofragment translational spectroscopy.

As with the then existing PTS methods,[8] the new variant recorded field-free time-of-flight (TOF) spectra of photofragments (H atoms in this case) formed by pulsed laser photolysis of the hydride molecule of interest (RH) seeded in a molecular beam, *i.e.*

$$\text{RH} + h\nu_{\text{phot}} \rightarrow \text{H} + \text{R}(E, v, N) \,, \tag{1}$$

where $h\nu_{\text{phot}}$ is the energy of the photolysis photon. The measured H atom TOF spectra were then transformed using energy and momentum conservation arguments to yield a spectrum of the total kinetic energy release (TKER) of the H + R fragments from which the energy disposal in the electronic (E), vibrational (v) and sometimes even the rotational (N) quantum states of the partner fragment (R) can be deduced, as well as the parent bond dissociation energy BDE_0(R–H). The novel feature was the method of detecting the H atom products, which were ionized at their point of creation using a two colour pulsed laser excitation scheme,

$$\text{H}(n = 1) + h\nu_1 \ (\tilde{\nu}_1 = 82259 \ \text{cm}^{-1}; \lambda_1 = 124.6 \ \text{nm}) \rightarrow \text{H}(n = 2) \tag{2a}$$

$$\text{H}(n = 2) + h\nu_2 \ (\tilde{\nu}_2 = 27420 \ \text{cm}^{-1}; \lambda_2 = 364.6 \ \text{nm}) \rightarrow \text{H}^+ + \text{e}, \tag{2b}$$

(where the λ_2 value quoted is the appropriate wavelength in air) and monitored via the TOF of the resulting ion.

H (and D) atoms have a pattern of energy levels familiar to all undergraduate chemists. To a very good approximation, the level energies only depend on the n quantum number and, via the Rydberg formula, the binding energy of an electron in the $n = 2$ level is just one quarter that of the electron in the $n = 1$ level. Thus the original experiments required just a single probe laser since the Lyman-α photons required for excitation (2a) could be conveniently generated by frequency tripling near UV laser light of the requisite frequency for the threshold ionization step (2b). As shown in Figure 1(a), for the specific case of H_2O photolysis at $\lambda = 125.1$ nm, the method was selective for H atoms (by virtue of the resonance enhanced ionization detection), sensitive, and afforded sufficient energy resolution to reveal that the partner OH products were indeed formed mainly in their ground (X) state, mainly in their $v = 0$ level, and with a highly excited, inverted, rotational state population distribution. This energy disposal was rationalised, qualitatively, by considering the topographies of the relevant excited state potential energy surfaces (PESs).[4] The observed high levels of fragment rotation explained the failure of all earlier efforts to monitor the OH(X) photoproducts by 'traditional' spectroscopy methods (*e.g.* laser induced fluorescence, LIF); the corresponding levels in the excited state of OH used in

4

the LIF detection scheme are heavily predissociated and have a negligible fluorescence quantum yield.

The study also served to highlight the universality of the method: Any photoinduced R–H (R–D) bond fission process was now potentially ripe for study, without requiring knowledge of a suitable and well characterised transition by which to probe the R co-fragment. The population distribution in the nascent R products is encoded in the H(D) atom TOF spectrum. Before summarising some of the many subsequent findings enabled by application of the technique – in studies of molecular photodissociation and of H/D atomic products from a range of bimolecular collision processes – we first describe the second generation variant of the experiment which remains the method of choice.

H (Rydberg) atom photofragment translational spectroscopy.

The original H_2O photolysis experiment defined a new 'gold standard' in terms of the achieved photofragment velocity resolution, but this was soon surpassed with the introduction of the H Rydberg atom (HRA) or 'Rydberg tagging' variant of PTS.[9,10] To appreciate the later advance it is first helpful to recognise the intrinsically low collection efficiency of the experiment. The photolysis and probe laser beams in most such photodissociation experiments counter-propagate with a narrow crossing angle along an axis at 90° to the molecular beam, and the H^+ ions are detected along a TOF axis orthogonal to the plane defined by the molecular and laser beams, as illustrated schematically in Figure 2(a). The detected signal intensity will be sensitive to the photofragment recoil anisotropy – *i.e.* the correlation between the recoil velocity and the polarization vector (ε_{phot}) of the photolysis photon, which is characterised by an anisotropy parameter, β. A key limitation, however, is that only a small fraction of the expanding Newton sphere of H atom fragments (of order a/S, where a and S are, respectively, the area of the detector and the surface area of the Newton sphere with radius equal to the distance between the interaction region and the front face of the detector) will strike the detector. Typically $a/S < 10^{-3}$ meaning that, for an isotropic recoil velocity distribution, less than one in every thousand H^+ ions formed in the interaction region will reach the detector. If anything, this analysis underestimates the total ion density created in the interaction volume, since one can envisage many routes whereby the photolysis and probe lasers may generate additional (heavier) ions. Given their mass (relative to that of the light H^+ ions), it is unlikely that these heavier ions would appear in the measured TOF spectrum, but the Coulombic

interactions between all of the charged particles at early times will inevitably cause some space

charge blurring of the photolysis-laser-induced H⁺ ion recoil velocity distributions of interest.

This limitation can be overcome if, rather than ionizing the H(D) atom products, the energy of the photon used in step (2b) is reduced slightly – *e.g.* to $\tilde{\nu}_2$ ~27410 cm^{-1} – so that the excitation from the $n = 2$ level now populates a high n Rydberg state of the neutral atom. An additional suitably timed probe laser pulse is now required, since the Lyman-α frequency (ν_1) is no longer equal to $3\nu_2$. Ions are still formed in the interaction region, but can be removed using a small DC field. This DC field,[10] and the fluctuating fields associated with the proximal charged particles,[11] are both thought to contribute to the l- and m_l-state mixing that is required in order that the lifetimes of the high n Rydberg states prepared by the resonance enhanced two photon excitation extend to the values deduced by experiment. The Rydberg tagged atoms are still ultimately detected as ions, but are only field ionized just before reaching the detector (*i.e.* after they have separated into their respective velocity sub-groups). Space charge broadening is no longer a first order impediment to product velocity resolution, so the photolysis and probe laser powers can be increased, with consequent benefits to signal intensity.

Applications in studies of molecular photodissociation processes

The Rydberg tagging method has provided new and detailed insights into the dissociation dynamics of numerous hydride molecules and radicals. These data have been central to recognising commonalities in the photofragmentation behaviour of families of molecules – that can be traced to similarities in the topographies of, and the non-adiabatic couplings between, the PESs sampled *en route* from the initial photoexcitation to the asymptotic products. The cross-sections for absorption to excited states formed by electron promotion to a σ^* antibonding orbital localised around the R–H bond of interest are often weak, but data generated by HRA-PTS studies allied with complementary theory [12,13] have promoted the now widespread recognition of the importance of such states in excited state bond fissions.[14-18] Here we highlight just a few examples.

HRA-PTS experiments have provided exquisitely detailed information concerning the energy disposal in the OH fragments formed in the photolysis of H_2O and its various isotopomers, at many different VUV wavelengths. [19 - 21] These data provide text-book illustrations of the increasing diversity of the couplings between excited states populated upon tuning to shorter wavelengths – reflecting the greater range of available fragmentation pathways at higher excitation energies. Figure 1(b), which shows TKER spectra derived from

H atom TOF measurements following photolysis of jet-cooled H_2O molecules at $\lambda = 123.94$

nm, serves to illustrate the current "state-of-the-art".[22] Both the VUV photolysis photons for

step (1) and the Lyman-α photons for step (2a) were provided by resonant four wave difference

frequency generation in a cell filled with Kr gas. Features associated with formation of H atoms

in tandem with numerous different v, N levels of the OH(A) and OH(X) partners are clearly

resolved. The energy resolution achieved (δ(TKER)/TKER ~0.3% at TKER = 10000 cm^{-1})

even allows population in different Λ-doublet states of the OH(X) products to be distinguished.

Analyses of such spectra also provide a direct determination of the parent dissociation energy,

e.g. BDE_0(H–OH) = 41145 cm^{-1}. [23]

The Rydberg tagging method has provided similarly detailed insights into photoinduced

S–H bond fission in H_2S at UV (200-250 nm) [24] and VUV (157.6 nm [25] and 121.6 nm [26])

excitation wavelengths, and N–H and C–H bond fissions in, respectively, NH_3 [27] and CH_4.[28,29]

The NH_2 and CH_3 fragments formed following excitation to the respective first excited singlet

states of NH_3 and CH_4 (both of which have 3s Rydberg character in the Franck-Condon region

but gain increasing σ^* antibonding valence character upon stretching the bond that eventually

breaks) are formed with substantial rotational excitation and, in both cases, the product recoil

anisotropy varies with the extent of this rotational excitation.

NH_3 photolysis at λ~216 nm, for example, yields H + $NH_2(\tilde{X})$ fragments. The latter are

formed in many different rotational levels, that span the entire range of available energies, E_{av}

(defined as the difference between ($hv_{phot} + E_{int}(NH_3)$) and BDE_0(H–NH_2)).[27] In all populated

levels, however, the rotational angular momentum is concentrated about the a-inertial axis of

the fragment. This specific angular momentum partitioning, and the product state dependent

recoil anisotropies, can be understood by recognising the competing nuclear motions during

the dissociation. First, we recognise that excitation with linearly polarised light aligns the

parent molecule in the laboratory frame and, if dissociation occurs on a timescale shorter than

that required for this alignment to be scrambled by parent rotation, this alignment will reveal

itself as an anisotropy of the product recoil velocities. The equilibrium geometries of the ground

and first excited states of NH_3 are, respectively, pyramidal and planar, and the parent transition

moment, μ, is directed along the C_3 rotation axis. Intuitively, therefore, we might anticipate a

negative recoil anisotropy parameter (*i.e.* that the departing H atoms recoil preferentially

perpendicular to μ), and such is indeed observed for the least rotationally excited $NH_2(\tilde{X})$

products. But the planar $\leftarrow$ pyramidal change in equilibrium geometry upon excitation prepares

7

molecules with out-of-plane bending vibrational motion orthogonal to the N–H bond fission coordinate. Any such out-of-plane motion will carry through into the dissociation products, in the form of a-axis rotation in the NH_2 product and orbital angular momentum of the H about the NH_2 – to the extent that the H atoms formed in association with the most rotationally excited $NH_2(\tilde{X})$ products exhibit a positive recoil anisotropy (*i.e.*, their recoil velocities are preferentially aligned parallel to μ and thus ε_{phot}).[27]

As noted above, the Rydberg tagging method offers exceptional TOF resolution, but low collection efficiencies. Thus the fact that the technique has been extensively applied to advance our understanding of the photofragmentation dynamics of small hydride molecules like H_2O, NH_3 and CH_4, should be no surprise. The radical fragments in these cases are sufficiently light, and their quantum states sufficiently separated in energy, that the challenge of working with small signals is more than compensated by the unprecedented resolution of the different H + R(E, v, N) product channels. This advantage starts to decline as we move to larger molecules that dissociate to yield heavier fragments, the quantum states of which cannot be fully resolved even by this high resolution PTS method. Even resolving the product vibrational states can reveal much about the fragmentation dynamics, however, as evidenced by UV photolysis studies of, for example, small polyatomic radicals like methyl,[30,31] ethyl,[32] vinyl [33] and allyl,[34] and heteroatom containing molecules like pyrrole,[35] imidazole,[36] phenol,[37] thiophenol,[38] and their substituted analogues.[39-41] The latter studies have encouraged some detailed comparisons of the fragmentation dynamics of these and related molecules following photoexcitation in the gas phase and when immersed in (weakly interacting) solvents.[42] They have also served to stimulate many complementary advances in the theoretical treatment of non-adiabatic transitions in excited state molecules.[43-49]

Applications in studies of bimolecular collision processes

The Rydberg tagging method has had similar impact in advancing studies of bimolecular collision processes in the gas phase. Again, Welge's group blazed the trail, with ground breaking studies of the hydrogen exchange reaction H + D_2 → HD + D at selected collision-energies.[10,50] The experiment involved two pulsed molecular beams – one of D_2, the other of HI seeded in a rare gas – propagating parallel to, but displaced from, each other as illustrated in Figure 2(b). Linearly polarized UV photolysis of HI yields H atoms with two narrowly defined velocity distributions (since the partner iodine atoms can be formed in their ground or excited spin-orbit state). This defined time zero for the encounters of interest. These velocity

sub-groups recoil at right angles to the beam propagation axis, but in orthogonal directions.

Thus by appropriate choice of the photolysis laser wavelength and polarization, H atoms with a single, tightly-defined spread of velocities can be arranged to intersect the beam of D_2 molecules, resulting in H + D_2 encounters with exquisitely controlled collision energies, E_{coll}. The D atom products were then Rydberg tagged after a short, user-defined time delay and their TOFs (and thus velocities) determined at different scattering angles to yield the first rovibrational state resolved differential cross-sections (DCSs) for the products of a bimolecular reaction. The success of these experiments encouraged more Rydberg tagging studies of the H + D_2 reaction at other E_{coll} values,[51-53] and of other isotopic variants of the hydrogen exchange reaction (*e.g.* H + HD,[52,54] D + H_2 [55]). Such data have provided a huge stimulus for high level theoretical studies of the H_3 PES and the nuclear motions it supports − studies that have identified reactive resonances and resonances associated with quantum bottleneck states, and have sought to identify definitive signatures for geometric phase effects.[56,57]

A variant of this experiment enabled dynamical studies of the H*(n) + D_2 → HD + D*(n') reaction (where H*(n) is a Rydberg excited H atom), and comparison with the analogous H^+ + D_2 ion-molecule reaction.[58-61] As in the H + H_2 ground state reaction studies (*vide supra*), the atomic reactants were formed with a tightly-defined velocity distribution by linearly polarized UV photolysis of HI. These H atoms were then Rydberg tagged at a well-defined time and location just before intersecting the beam of D_2 molecules and the rotationally resolved product distribution was derived from the TOF distributions of the Rydberg atoms (RAs) measured at a number of different scattering angles.

Similar studies followed not only for isotopic variants of this reaction,[62,63] but also for the inelastic scattering of hydrogen RAs with N_2 [64] and O_2,[64,65] at more than one collision energy. The H*($n = 46$) + O_2($v = 0, N = 1, 3$) studies revealed some propensity for very large translation to vibration energy transfers. For example, >90% of the incident kinetic energy must transfer into product vibration in order to form the back scattered O_2($v' = 8$) products observed at E_{coll} = 1.55 eV.[65] (Backwards is here defined relative to the incident direction of the H*($n = 46$) atoms). Such observations can be understood, qualitatively at least, by invoking an initial charge transfer from the (proton) core to the O_2. But more recent studies for **H***($n = 46$) atom scattering off HD($v = 0, J = 0$) molecules at E_{coll} = 0.5 eV, for example, run counter to this conclusion. Analysis of the latter data revealed contributions from elastic/inelastic and reactive processes yielding, respectively, **H***(n') + HD(v', J'), and both H*(n') + **H**D(v', J') and D*(n') + **H**H(v', J') products.[62] (A bold font here identifies the incident Rydberg atom, and bold italic

font is used to identify that atom in the products). The angular distribution of the total H_2 product yield shows preferential forward/backward scattering – in marked contrast to that predicted for the corresponding ion-molecule reaction. The validity, or otherwise, of neglecting the coupling between the ion core and the Rydberg electron in such RA–molecule collisions remains an open question.

We now highlight other instances where Rydberg tagging methods have been used to derive high resolution speed and angular distributions of H(D) atom products from prototypical bimolecular reactions.[66] The reaction of electronically excited $O(^1D)$ atoms with H_2 molecules, for example, is important in atmospheric chemistry and is frequently touted as a text-book example of a reaction occurring via an insertion mechanism.[67] Analysis of structure in the TOF spectra of the H atom products measured (after Rydberg tagging) at different scattering angles allowed determination of the OH (v', N') product state resolved DCSs at one collision energy (E_{coll} = 1.3 kcal mol^{-1}, 0.056 eV) [68] and investigation of how the reaction dynamics are affected by rotational excitation [69] and deuteration of the molecular reactant.[70-72] The state resolved DCSs derived from these studies are consistent with an insertion mechanism at low E_{coll}, but reveal the growing importance of a rival abstraction mechanism at higher collision energies.

The F + H_2 reaction has also long been regarded as a benchmark system – a prototypical exothermic reaction, with an 'early' transition state favouring direct abstraction of an H atom and backward scattering of the HF products.[73] Interest in this reaction was heightened by early predictions that it should support reactive scattering resonances,[74,75] *i.e.* short-lived, quasi-bound quantum states that are formed and decay during the course of the evolution from reactants to H + HF products. Detecting and characterising these resonances should provide a particularly direct probe of the transition state region of the PES for the reaction. Crossed molecular beam (CMB) experiments of the F + H_2 reaction, with mass spectrometric product detection, afforded the first experimental demonstration of such a resonance – a striking forward scattered peak for the HF(v'= 3) products.[76]

CMB methods coupled with Rydberg tagging of the H (and D) atom products have since enabled determination of rovibrational product state resolved DCSs for the reaction of F atoms with $H_2(v = 0)$ at E_{coll} = 0.52 kcal mol^{-1} (0.023 eV) [77] and $H_2(v = 1, J = 0)$ at energies in the range 0.4 to 2.0 kcal mol^{-1} (0.017-0.087 eV),[78] and for the D atom products arising in the reaction of F atoms with HD($v = 0$, $J = 0$) and HD($v = 1$, $J = 0$) at various energies in the respective ranges E_{coll} = 0.9-1.5 kcal mol^{-1} (0.039-0.065 eV) [79,80] and 0.2-0.8 kcal mol^{-1} (0.009-0.035 eV).[81] In each case, the measurements were complemented by 3-D quantum dynamics

calculations on the best available PES yielding a 'whole' that is greater than the sum of the parts. The measurements ultimately serve to test and validate the accuracy of the *ab initio* PES, while the calculations provide insights and interpretations for the experimental observations and allow prediction of hitherto unobserved phenomena.

The data for the F + $H_2(v = 0, 1; J = 0)$ reaction shown in Figure 3 illustrate the merits of this fusion of high level experiment and theory. Figure 3(a) shows TOF spectra of the (Rydberg tagged) H atom products formed at a low collision energy, $E_{coll} = 0.023$ eV, with and without the stimulated Raman (SR) pumping used to pre-excite a fraction of the H_2 reagent molecules to their $v = 1; J = 0$ level. These data were measured at laboratory scattering angles that approximate to the backward (180°, relative to the F atom beam) and forward (0°) directions in the centre of mass frame. These TOF spectra show structure that reveals the rovibrational state population distributions in the HF partner. HF($v' = 2$) products from F + $H_2(v = 0, J = 0)$ collisions are clearly evident at both scattering angles, whereas HF($v' = 3$ and 4) products are only visible from the F + $H_2(v = 1; J = 0)$ reaction, and only in the backward direction.

Rovibrational product state resolved DCSs for the reaction of F atoms with $H_2(v = 0, J = 0)$ and $H_2(v = 1, J = 0)$ molecules at $E_{coll} = 0.023$ eV derived from measurements at many scattering angles are shown in Figure 3(b), along with the corresponding theoretical predictions. Clearly, the agreement between experiment and theory is excellent. The forward scattered HF($v' = 2$) product peak, which theory identifies as a Feshbach resonance in the F + $H_2(v = 0)$ reaction path, is absent in the F + $H_2(v = 1)$ reaction, though back-scattered HF($v' = 2$, 3 and 4) products are clearly discernible from this latter reaction.[77] The vibrationally adiabatic potentials (VAPs) shown in Figure 3(c) provide a qualitative rationale for the observed product state distributions, and their dependence on reagent vibration.[79] The asymptotic energy of the F + $H_2(v = 0, J = 0)$ reaction is below that of the H + HF($v' = 3$) products, but the VAP shows a shallow well in the H….HF($v' = 3$) coordinate and the reaction probability will increase whenever E_{coll} matches with one of these post-barrier Feshbach resonance states. The decay of one such resonance is responsible for the forward peaking HF($v' = 2$) products in Figure 3(b). The asymptotic energy of the F + $H_2(v = 1; J = 0)$ reactants, in contrast, lies well above that of the H + HF($v' = 4$) products – which rules out the possibility of similar reactive resonances in F + $H_2(v = 1; J = 0)$ collisions and explains the preponderance of back scattered HF products. Questions remain, however. Careful inspection of the DCSs shown in Figure 3(b) reveals a small forward peaking HF($v' = 4$) yield from the F + $H_2(v = 1; J = 0)$ reaction. The relative

importance of this feature increases rapidly with increasing E_{coll}, but the dynamical origin of these products has still to be established.

CMB methods coupled with Rydberg tagging of the H atom products have also been applied to the Cl + HD($v = 1$, $J = 0$)) $\rightarrow$ DCl(v') + H reaction.[82] The DCl products are predominantly back-scattered, but the differential cross-section for forming back-scattered DCl($v' = 1$) products shows clear maxima at $E_{coll} = 2.4$ and 4.3 kcal mol^{-1} (0.10 and 0.19 eV). Again, quantum dynamics calculations on an accurate PES suggest that these features may be attributed to very short lived dynamical resonances trapped in the post-barrier well on the H….DCl($v' = 2$) VAP arising from bond-softening, *i.e.* from dynamical effects reminiscent of those outlined for the F + HD($v = 1$, $J = 0$) reaction in Figure 3.

The benefits of Rydberg tagging in experiments of this type are not limited to three atom reactions. CMB studies of the OH + D$_2$ [83,84] and OH + HD [85] reactions have been reported with Rydberg tagging of the D atom products. In the former reaction, for example, DCSs have been determined at $E_{coll} = 0.25$, 0.28 and 0.34 eV, along with the E_{coll} dependence of the DCS in the backward direction. The DCSs are dominated by backward scattering, consistent with a direct rebound mechanism, and show clear peaks consistent with formation of HOD products with, respectively, one and two quanta of O–D stretching vibration. These experimental findings are reproduced well by contemporary theory using the best available PESs for the OH + H$_2$ system.[84,86] Theory can also predict how vibrational excitation of the OH reactant would manifest in the HOD product vibrations [86] – a challenge that, in the case of this particular reaction, has yet to be addressed by experiments.

A prospective view

Most photodissociation dynamics studies of small gas phase molecules reported to date have employed UV excitation wavelengths. This choice has some logic, in as much that the photoexcitation populates (relatively) low lying excited electronic states and only a small number of fragmentation pathways are energetically accessible. Thus the electronic structure and molecular dynamics calculations required to guide interpretation of data from such experiments (including adequate treatment of non-adiabatic effects) are often tractable. This complementarity between experiment and theory becomes increasingly challenged as we move to shorter excitation wavelengths, and the range of excited states, non-adiabatic couplings and fragmentation pathways all increase. But there are also practical reasons for the historic bias in favour of UV excitations. The sources of suitably intense, pulsed VUV radiation suitable for

photodissociation dynamics experiments have traditionally been limited to excimer lasers (*e.g.* ArF at 193 nm, or the F_2 laser at 157.6 nm). Only recently, with the advent of efficient table-top four wave sum and difference frequency schemes and dedicated FEL-based VUV sources like that at the DCLS (Dalian Coherent Light Source) [21, 87] has it become realistic to contemplate conducting molecular photodissociation experiments at any user selected excitation wavelength longer than ~50 nm, *i.e.* at wavelengths below the LiF cut-off and above the ionization limit of almost all molecules. Thus we can anticipate many more carefully targeted molecular photofragmentation and photoionization studies at these shorter excitation wavelengths, and that H/D Rydberg tagging methods will play a central role in probing the dynamics of photoinduced dissociations yielding electronically excited R co-fragments, or R^+ co-fragments in the case of dissociative ionization processes, or multiple fragments when exciting at energies above the three body dissociation limit.

The UV photolysis of hydrogen halide molecules has already featured in this Perspective: HI(DI) photolysis is the favoured route to forming H(D) atom reactants with well-defined velocity distributions for inelastic and reactive gas phase scattering studies. Similar considerations have guided the choice of HI(DI) photolysis as the source, and Rydberg tagging as the probe, for studies of the inelastic scattering of H(D) atoms off well-characterised metal surfaces at collision energies in the range 1-3 eV. [88, 89] These experiments, along with complementary modelling, have shown that incident KE is lost in exciting electron-hole pairs, with an efficiency that depends much more on the coupling to phonon modes (*i.e.* to the ratio of the masses of the incident and the surface metal atoms) than on the detailed electronic structure.[89] The H(D) atom sticking probability is deduced to be greater for near normal incidence collisions − consistent with a mechanism whereby accommodation involves the incident atom first penetrating the surface then resurfacing.[88]

HBr photolysis at 212.8 nm has been used to demonstrate spin-polarized HRA TOF spectroscopy.[90,91] These studies show how, by appropriate choice of experimental geometry and laser polarizations for the double resonant excitation scheme (2), it is possible to fully determine the (velocity dependent) spin distribution of the H atom product − which can be a sensitive reporter of the non-adiabatic dynamics involved in its formation.

Looking forward, with the advent of dedicated FEL-based VUV radiation sources, we can anticipate that short wavelength photolysis of HI(DI), for example, will find use as a source of H(D) atoms with hyperthermal translational energies in the range of 5-8 eV. The inelastic and reactive scattering of H(D) atoms at such high collisional energies should offer many new

insights into non-adiabatic dynamics (*e.g.*, geometric phase effects) involving excited state PESs.

This Perspective is not intended to be a comprehensive review but, for completeness, we note a couple of limitations of the Rydberg tagging method. First, it is (mainly) limited to probing H and D atoms. A similar two photon, two colour double resonance excitation scheme has been used to prepare high *n* Rydberg states of atomic oxygen, and to monitor the KE distributions (by TOF methods) of $O(^3P)$ atom products from the 355 nm photodissociation of NO_2 [92] and, in a CMB study, from the $CN + O_2$ reaction.[93] High *n* Rydberg states of O and S atoms have also been prepared by single (VUV) photon excitation, and used in PTS studies of the $O(^3P_2)$ atoms resulting from 193 nm photolysis of SO_2 and the $S(^3P_2)$ products of the 202.3 nm photodissociation of CS_2.[94] These are rare exceptions, however. The second limitation of all Rydberg tagging methods is the (necessarily high) energy of the probe photons. The act of focussing the probe beam(s) into a small interaction region can – particularly in the case of larger molecules – cause unintended (but often unavoidable) photochemistry additional to that which they are intended to probe. These caveats aside, it is clear that Rydberg tagging methods have made, and will continue to make, very substantial contributions to advancing our knowledge and understanding in many areas of photoinitiated molecular reaction dynamics.

Acknowledgements

Figure Captions

Figure 1

(a) The first TKER spectrum of H+OH products from the photodissociation of jet-cooled H_2O molecules at $\lambda = 125.1$ nm using H^+ ion detection. (Adapted from ref. 4 by permission of the Royal Society of Chemistry (RSC). (b) TKER spectrum of the same products formed by 123.94 nm photolysis of jet-cooled H_2O molecules, derived from a HRA-TOF spectrum measured along the axis parallel to ε_{phot} (adapted from Ref. 22, copyright 2008 National Academy of Sciences.).

Figure 2

Schematic showing the molecular beam and detection (TOF) axes for (a) standard photodissociation and (b) crossed-beam reactive scattering experiments employing Rydberg tagging to detect the H atom products. The photolysis and tagging lasers in both cases are incident along the axis perpendicular to the plane of the figure.

Figure 3

(a) TOF spectra of (Rydberg tagged) H atom products from the $F + H_2(v = 0, J = 0)$ (blue) and $F + H_2(v = 1, J = 0)$ (red) reactions at $E_{coll} = 0.023$ eV. The data were recorded at laboratory scattering angles that approximate the backward (180°, relative to the F atom beam) and forward (0°) directions in the centre of mass frame. (b) Contour plots comparing the experimentally derived (left) and the calculated (right) rovibrational product state resolved DCSs for the $F + H_2(v = 0, J = 0)$ and $F + H_2(v = 1, J = 0)$ reactions at this collision energy (upper and lower rows, respectively). (c) Schematic illustration of the first few vibrationally adiabatic potentials for the $F + H_2$ reaction (adapted with permission from ref. 78. Copyright 2015 American Chemical Society).
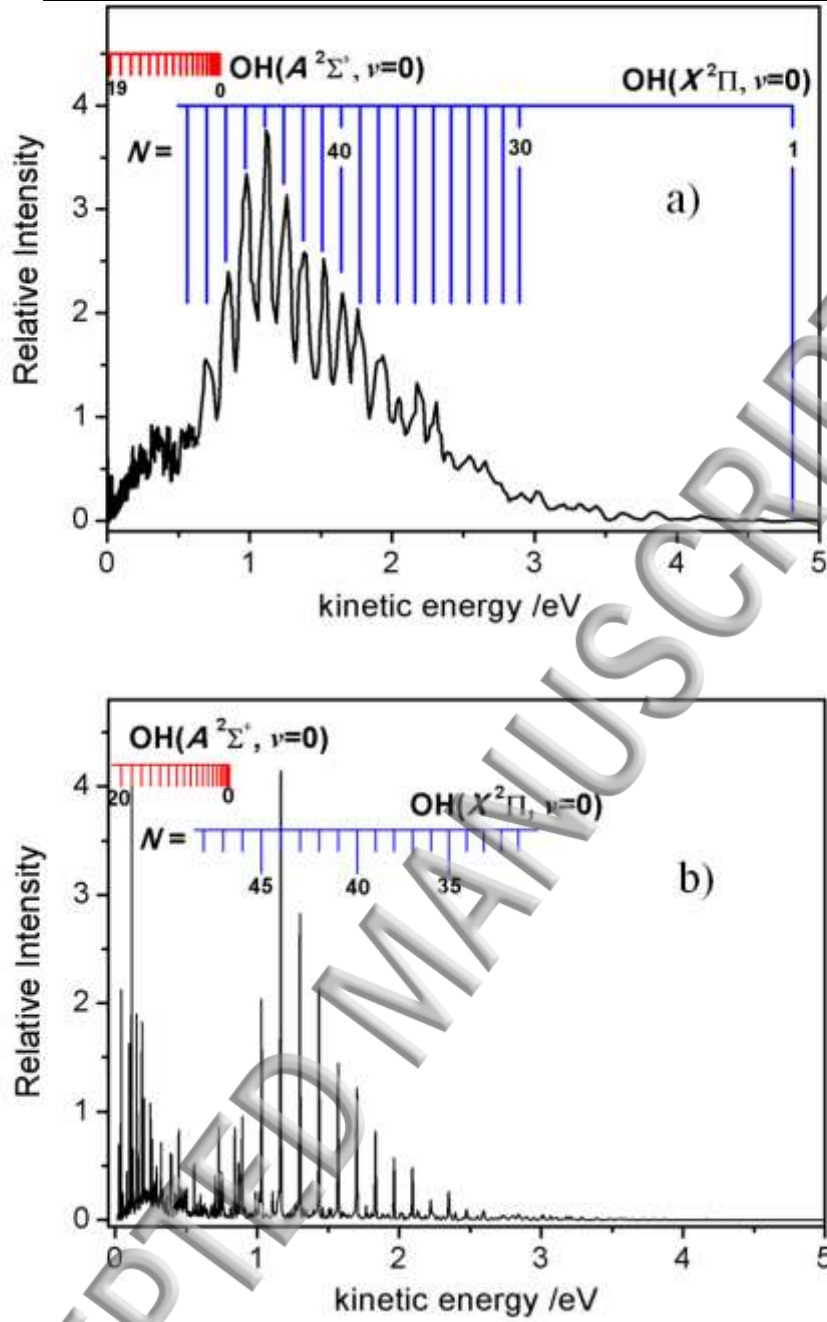
Figure 1

a)

Signal

-200 VDC
-2500 VDC

MCP Z STACK
Grid

H*(n)

Pulsed valve

Photodissociation/
Rydberg tagging region

H_2O/Ar

b)

Rotatable
MCP detector

D*(n)

H or O(^{1}D)

Pulsed Valve 1

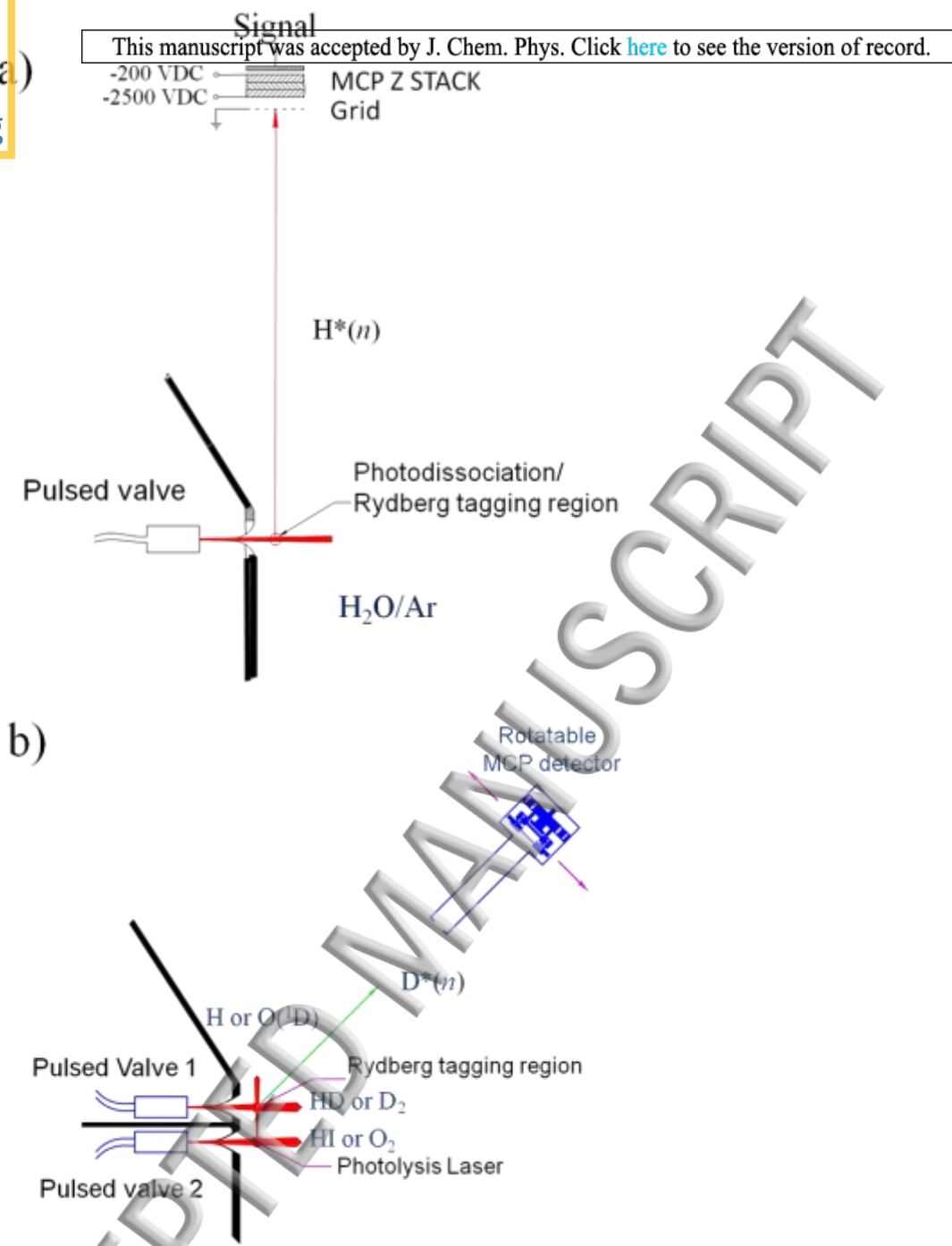Rydberg tagging region

HD or D_2

HI or O_2

Photolysis Laser

Pulsed valve 2

Figure 2

Figure 3

References

[1] D.W. Chandler, P.L. Houston and D.H. Parker, *J. Chem. Phys*. **147**, 013601 (2017).

[2] A.T.J.B. Eppink and D.H. Parker, *Rev. Sci. Instrum*. **68**, 3477 (1997).

[3] D.W. Chandler and P.L. Houston, *J. Chem. Phys*. **87**, 1445 (1987).

[4] H.J. Krautwald, L. Schnieder, K.H. Welge and M.N.R. Ashfold, *Farad. Disc. Chem. Soc.,* **82**, 99 (1986).

[5] M.N.R. Ashfold, J.M. Bayley and R.N. Dixon, *Chem. Phys*., **84**, 35 (1984).

[6] T. Carrington, *J. Chem. Phys*. **41**, 2012 (1964).

[7] T.G. Slanger and G. Black, *J. Chem. Phys.,* **77**, 2432 (1982).

[8] K.R. Wilson, in *Symposium on Excited State Chemistry,* ed. J.N. Pitts, Jr. (Gordon and Breach, New York, 1970)

[9] L. Schnieder, W. Meier, K.H. Welge, M.N.R. Ashfold and C.M. Western, *J. Chem. Phys*. **92**, 7027 (1990).

[10] L. Schnieder, K. Seekamp-Rahn, E. Wrede and K.H.Welge, *J. Chem. Phys*. **107**, 6175 (1997).

[11] F. Merkt and R.N. Zare, *J. Chem. Phys*. **101**, 3495 (1994).

[12] A.L. Sobolewski, W. Domcke, C. Dedonder-Lardeux and C. Jouvet, *Phys. Chem. Chem. Phys.* **4**, 1093 (2002).

[13] W. Domcke and D.R. Yarkony, *Ann. Rev. Phys. Chem*. **63**, 325 (2012).

[14] M.N.R. Ashfold, B. Cronin, A.L. Devine, R.N. Dixon and M.G.D. Nix, *Science* **312**, 1637 (2006).

[15] M.N.R. Ashfold, G.A. King, D. Murdock, M.G.D. Nix, T.A.A. Oliver and A.G. Sage, *Phys. Chem. Chem. Phys*. **12**, 1218 (2010).

[16] G.M. Roberts and V.G. Stavros, *Chem. Sci*. **5**, 1698 (2014).

[17] M.N.R. Ashfold, D. Murdock and T.A.A. Oliver, *Ann. Rev. Phys. Chem*. **68**, 63 (2017).

[18] M.N.R. Ashfold, R.A. Ingle, T.N.V. Karsili and J.S. Zhang, *Phys. Chem. Chem. Phys*. (submitted).

[19] R.N. Dixon, D.W.H. Hwang, X.F. Yang, S.A. Harich, J.J. Lin and X.M.Yang, *Science* **285**, 1249 (1999).

[20] K.J. Yuan, R.N. Dixon and X.M. Yang, *Acc. Chem. Res*. **44**, 369 (2011) and references therein.

[21] H.L. Wang, Y. Yu, Y. Chang. S. Su, S.R. Yu, Q.M. Li, K. Tao, H.L. Ding, J. Yang, G.L. Wang, L. Che, Z.G. He, Z.C. Chen, X. Wang, W. Zhang, D.X. Dai, G.R. Wu, K.J. Yuan and X.M. Yang, *J. Chem. Phys.* **148**, 124301 (2018).

[22] K.J. Yuan, Y. Cheng, L. Cheng, Q. Guo, D.X. Dai, X.Y. Wang, X.M. Yang and R.N. Dixon, *Proc. Natl. Acad. Sci. U.S.A.* **105**, 19148 (2008).

[23] B. Ruscic, *J. Phys. Chem*. *A* **119**, 7810 (2015).

[24] S.H.S. Wilson, J.D. Howe and M.N.R. Ashfold, *Mol. Phys.* **88**, 841 (1996).

[25] X. Liu, D.W. Hwang, X.F. Yang, S. Harich, J.J. Lin and X. Yang, *J. Chem. Phys.* **111**, 3940 (1999).

[26] P.A. Cook, S.R. Langford, R.N. Dixon and M.N.R. Ashfold, *J. Chem. Phys.* **114**, 1672 (2001).

[27] D.H. Mordaunt, M.N.R. Ashfold and R.N. Dixon, *J. Chem. Phys*. **104**, 6460 (1996); **109**, 7659 (1998).

[28] D.H. Mordaunt, I.R. Lambert, G.P. Morley, M.N.R. Ashfold, R.N. Dixon, C.M. Western, L. Schnieder and K.H. Welge, *J. Chem. Phys.* **98**, 2054 (1993).

[29] Y.W. Zhang, K.J. Yuan, S.R. Yu and X.M. Yang, *J. Phys. Chem. Letts*. **1**, 475 (2009).

[30] S.H.S.Wilson, J.D. Howe, K.N. Rosser, M.N.R. Ashfold and R.N. Dixon, *Chem. Phys. Lett.* **227**, 456 (1994).

[31] G.R. Wu, B. Jiang, Q. Ran, J.H. Zhang, S.A. Harich and X.M. Yang, *J. Chem. Phys.* **120**, 2193 (2004).

[32] G. Amaral, K.S. Xu and J.S. Zhang, *J. Chem. Phys.* **114**, 5164 (2001).

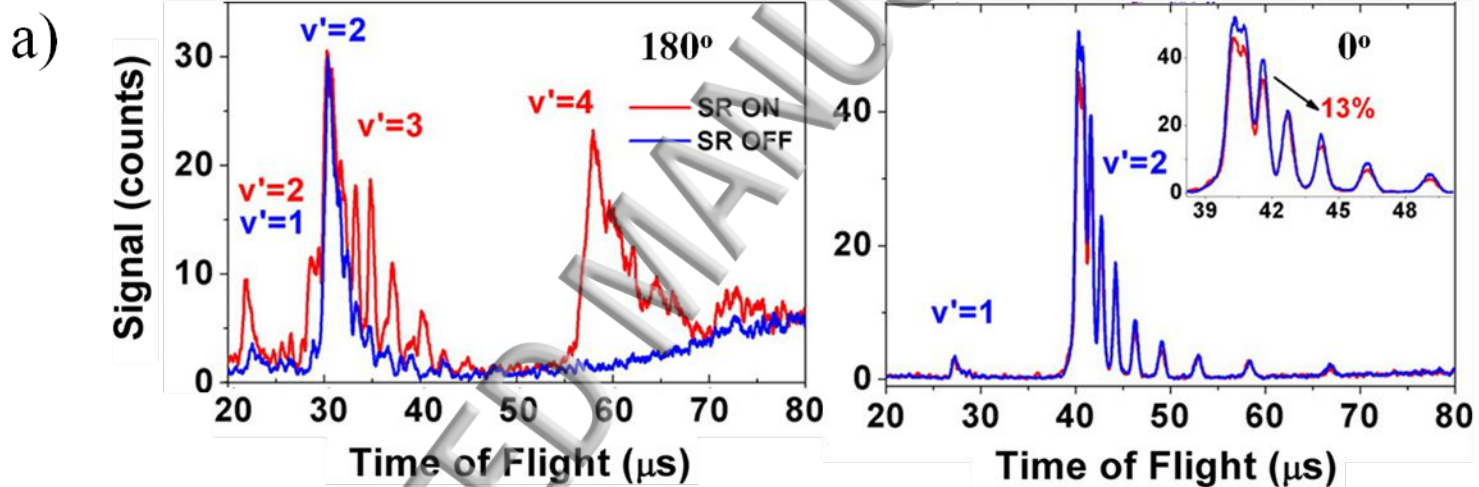[33] K.S. Xu and J.S. Zhang, *J. Chem. Phys.* **111**, 3783 (1999).

[34] Y. Song, M. Lucas, M. Alcaraz, J.S. Zhang and C. Brazier, *J. Phys. Chem. A* **119**, 12318 (2015).

[35] B. Cronin, M.G.D. Nix, R.H. Qadiri and M.N.R. Ashfold, *Phys. Chem. Chem. Phys.* **6**, 5031 (2004).

[36] A.L. Devine, B. Cronin, M.G.D. Nix and M.N.R. Ashfold, *J. Chem. Phys.* **125**, 184302 (2006).

[37] M.G.D. Nix, A.L. Devine, B. Cronin, R.N. Dixon and M.N.R. Ashfold, *J. Chem. Phys.* **125**, 133318 (2006).

[38] A.L. Devine, M.G.D. Nix, R.N. Dixon and M.N.R. Ashfold, *J. Phys. Chem. A* **112**, 9563 (2008).

[39] T.N.V. Karsili, B. Marchetti, R. Moca and M.N.R. Ashfold, *J. Phys. Chem. A*. **117**, 12067 (2013).

[40] T.N.V. Karsili, A.M. Wenge, D. Murdock, S.J. Harris, J.N. Harvey, R.N. Dixon and M.N.R. Ashfold, *Chem. Sci.* **4**, 2434 (2013).

[41] T.A.A. Oliver, G.A. King, D.P. Tew, R.N. Dixon and M.N.R. Ashfold, *J. Phys. Chem. A* **116**, 12444 (2012).

[42] S.J. Harris, D. Murdock, Y. Zhang, T.A.A. Oliver, M.P. Grubb, A.J. Orr-Ewing, G.M. Greetham, I.P. Clark, M. Towrie, S.E. Bradforth and M.N.R. Ashfold, *Phys. Chem. Chem. Phys.* **15**, 6567 (2013).

[43] V. Vallet, Z.G. Lan. S. Mahapatra, A.L. Sobolewski and W. Domcke, *J. Chem. Phys.* **123**, 144307 (2005).

[44] Z.G. Lan, W. Domcke, V. Vallet, A.L. Sobolewski and S. Mahapatra, *J. Chem. Phys.* **122**, 224315 (2005).

[45] R.N. Dixon, T.A.A. Oliver and M.N.R. Ashfold, *J. Chem. Phys.* **134**, 194303 (2011).

[46] D.V. Makhov, K. Saita, T.J. Martinez and D. Shalashilin, *Phys. Chem. Chem. Phys.* **17**, 3316 (2015).

[47] H. Guo and D.R. Yarkony, *Phys. Chem. Chem. Phys.* **18**, 26335 (2016).

[48] C.J. Xie, J.Y. Ma, X.L. Zhu, D.R. Yarkony, D.Q. Xie and H. Guo, *J. Amer. Chem. Soc*. **138**, 7828 (2016).

[49] D. Picconi and S.Yu. Grebenshchikov, *J. Chem. Phys.* **148**, 104103 (2018); **148**, 104104 (2018).

[50] E. Wrede, L. Schnieder, K.H. Welge, F.J. Aoiz, L. Banares, J.F. Castillo, B. Martinez-Haya and V.J. Herrero, *J. Chem. Phys*. **110**, 9971 (1999).

[51] S.A. Harich, D. Dai, X. Yang, S.D. Chao and R.T. Skodje, *J. Chem. Phys.* **116**, 4769 (2002)

[52] S.D. Chao, S.A. Harich, D. Dai, C.C. Wang, X. Yang and R.T. Skodje, *J. Chem. Phys.* **117**, 8341 (2002).

[53] D. Dai, C.C. Wang, S.A. Harich, X. Wang and X. Yang, S.D. Chao and R.T. Skodje, *Science* **300**, 1730 (2003).

[54] S.A. Harich, D. Dai, C.C. Wang, X. Yang, S.D. Chao and R.T. Skodje, *Nature* **419**, 281 (2002).

[55] J. Zhang, D. Dai, C.C. Wang, S.A. Harich, X. Wang and X. Yang, *Phys. Rev. Lett.* **96**, 093201 (2006).

[56] X.M. Yang, *Phys. Chem. Chem. Phys.* **13**, 8112 (2011) and references therein.

[57] J. Jankunas, M. Sneha, R.N. Zare, F. Bouakline, S.C. Althorpe, D. Herraez-Anguila and F.J. Aoiz, *Proc. Nat. Acad. Sci. USA* **111**, 15 (2014) and references therein.

[58] D. Dai, C.C. Wang, G. Wu, S.A. Harich, H. Song, M. Hayes, R.T. Skodje, X. Wang, D. Gerlich and X. Yang, *Phys. Rev. Lett.* **95**, 013201 (2005).

[59] E. Wrede, L. Schnieder, K. Seekamp-Rahn, B. Niederjohann and K.H. Welge, *Phys. Chem. Chem. Phys.* **7**, 1577 (2005).

[60] H. Song, D.X. Dai, G.R. Wu, C.C. Wang, S.A. Harich, M.Y. Hayes, X.Y. Wang, D. Gerlich, X.M. Yang and R.T. Skodje, *J. Chem. Phys.* **123**, 074314 (2005).

[61] S.R. Yu, K.J. Yuan, H. Song, X. Xu, D.X. Dai, D.H. Zhang and X.M. Yang, *Chem. Sci.* **3**, 2839 (2012).

[62] S.R. Yu, S. Su, D.X. Dai, K.J. Yuan and X.M. Yang, *J. Chem. Phys.* **140**, 034310 (2014).

[63] S.R. Yu, S. Su, D.X. Dai, K.J. Yuan and X.M. Yang, *Phys. Chem. Chem. Phys.* **17**, 9659 (2015).

[64] B.S. Strazisar, C. Lin and H.F. Davis, *Phys. Rev. Lett.* **86**, 3997 (2000).

[65] S.R. Yu, S. Su, K.J. Yuan, D.X. Dai and X.M. Yang, *J. Phys. Chem. Lett.* **3**, 2420 (2012).

[66] X.M. Yang, *Int. Rev. Phys. Chem.* **24**, 37 (2005).

[67] P. Casavecchia, *Rep. Prog. Phys.* **63**, 355 (2000).

[68] X. Liu, J.J. Lin, S. Harich, G.C. Schatz and X. Yang, *Science*, **289**, 1536 (2000).

[69] X. Liu, C.C. Wang, S.A. Harich and X. Yang, *Phys. Rev. Lett.* **89**, 133201 (2002).

[70] X. Liu, J.J. Lin, S.A. Harich and X. Yang, *J. Chem. Phys.* **113**, 1325 (2000).

[71] X. Liu, J.J. Lin, S. Harich and X. Yang, *Phys. Rev. Lett.* **86**, 408 (2001).

[72] K. Yuan, Y. Chen, X. Liu, J.J. Lin, S.A. Harich, X. Yang and D. Zhang, *Phys. Rev. Lett.* **96**, 103202 (2006).

[73] Z.F. Ren, Z.G. Sun, D.H. Zhang and X.M. Yang, *Rep. Prog. Phys.* **80**, 026401 (2017) and references therein.

[74] S.-F. Wu, B.R. Johnson and R.D. Levine, *Mol. Phys.* **25**, 839 (1973).

[75] G.C. Schatz, J.M. Bowman and A. Kuppermann, *J. Chem. Phys.* **58**, 4023 (1973); 6**3**, 674 (1975).

[76] D.M. Neumark, A.M. Wodtke, G.N. Robinson, C.C. Hayden and Y.T. Lee, *J. Chem. Phys.* **82**, 3045 (1985).

[77] M. Qiu, Z. Ren, L. Che, D. Dai, S.A. Harich, X. Wang, X. Yang, C. Xu, D. Xie, M. Gustafsson, R.T. Skodje, Z. Sun and D.H. Zhang, *Science* **311**, 1440 (2006).

[78] T.G. Yang, L. Huang, T. Wang, C.L. Xiao, Y. Xie, Z.G. Sun, D.X. Dai, M. Chen, D.H. Zhang and X. Yang, *J. Phys. Chem. A* **119**, 12284 (2015).

[79] Z. Ren, L. Che, M. Qiu, X. Wang, W. Dong, D.X. Dai, X. Wang, X.M. Yang, Z.G. Sun, B. Fu, S.-Y. Lee, X. Xu and D.H. Zhang, *Proc. Nat. Acad. Sci. USA* **105**, 12662 (2008).

[80] W. Dong, C.L. Xiao, T. Wang, D.X. Dai, X. Yang and D.H. Zhang, *Science* **327**, 1501 (2010).

[81] T. Wang, J. Chen, T.G. Yang, C.L. Xiao, Z.G. Sun, L. Huang, D.X. Dai, X. Yang and D.H. Zhang, *Science* **342**, 1499 (2013).

[82] T.G. Yang, J. Chen, L. Huang, T. Wang, C.L. Xiao, Z.G. Sun, D.X. Dai, X.M. Yang and D.H. Zhang, *Science* **347**, 60 (2015).

[83] B.R. Strazisar, C. Liu and H.F. Davis, *Science* **290**, 958 (2000).

[84] S. Liu, C.L. Xiao, T. Wang, J. Chen, T.G. Yang, X. Xu, D.H. Zhang and X.M. Yang, *Farad. Disc.* **157**, 101 (2012).

[85] C. Xiao, X. Xu, S. Liu, T. Wang, W. Dong, T. Yang, Z. Sun, D. Dai, D.H. Zhang and X. Yang, *Science* **330**, 440 (2011).

[86] B. Zhao, Z.G. Sun and H. Guo, *J. Chem. Phys.* **145**, 134308 (2016).

[87] Y. Chang, S. R.Yu, Q. Li, Y. Yu, H. Wang, S. Su, Z. C. Chen, L. Che, X. Wang, W. Zhang, D. X. Dai, G. Wu, K. J. Yuan and X. M. Yang, *Rev. Sci. Instrum.*, **89**, 063113 (2018).

[88] O. Bünermann, H.Y. Jiang, Y. Dorenkamp, A. Kandrstsenka, S.M. Janke, D.J. Auerbach and A.M. Wodtke, *Science* **350**, 1346 (2015).

[89] Y. Dorenkamp, H.Y. Jiang, H.J. Köckert, N. Hertl, M. Kammler, S.M. Janka, A. Kandrstsenka, A.M. Wodtke and O. Bünermann, *J. Chem. Phys.* **148**, 034706 (2018).

[90] B.M. Broderick, Y.M. Lee, M.B. Doyle, V.Y. Chernyak, O.S. Vasyutinskii and A.G. Suits, *Rev. Sci. Instrum.* **85**, 053103 (2014).

[91] B.M. Broderick, A.G. Suits and O.S. Vasyutinskii, *J. Chin. Chem. Soc.* **64**, 877 (2017).

[92] C. Lin, M.F. Witinski and H.F. Davis, *J. Chem. Phys.* **119**, 251 (2003).

[93] M.F. Witinski, M. Ortiz-Suárez and H.F. Davis, *J. Chem. Phys.* **124**, 094307 (2006).

[94] B. Jones, J.G. Zhou, L. Yang and C.Y. Ng, *Rev. Sci. Instrum.* **79**, 123106 (2008).

a)

Relative Intensity

OH($A\ ^2\Sigma^+$, v=0)

19   0

OH($X\ ^2\Pi$, v=0)

N =

40   30   1

kinetic energy /eV

b)

Relative Intensity

OH($A\ ^2\Sigma^+$, v=0)

20   0

OH($X\ ^2\Pi$, v=0)

N =

45   40   35

kinetic energy /eV

a)

Signal

-200 VDC
-2500 VDC
Grid

MCP Z STACK

H*(n)

Pulsed valve

Photodissociation/
Rydberg tagging region

H_2O/Ar

b)

Rotatable
MCP detector

H or $O(^1D)$

D*(n)

Pulsed Valve 1

Rydberg tagging region

HD or D_2

HI or O_2

Pulsed valve 2

Photolysis Laser

a)

180° — SR ON (red), SR OFF (blue)

v'=2, v'=3, v'=4, v'=1

0° — 13%

v'=2, v'=1

b)

Exp(0.023eV)   Theory(0.023eV)

HF(v'=3)
F(²P₃/₂)
HF(v'=1)
HF(v'=2)
H₂(v=0, j=0)

HF(v'=4)
F(²P₃/₂)
HF(v'=2)
HF(v'=3)
H₂(v=1, j=0)

c)

$H_2(v=1)+F$ E_c v'=4

$H_2(v=0)+F$ (004) (104)   v'=3

(003)   v'=2

Strong Coupled Region   v'=1

v'=0

$HF(v')+H$

Reaction Coordinate